

# Wearable Sensor Framework for Rehabilitation Monitoring Following Knee-Related Conditions

Can Tekdemir<sup>1</sup>, Yusuf Ziya Hayirlioglu<sup>1</sup>, Olgar Birsnel<sup>2</sup><sup>a</sup> and Beren Semiz<sup>1</sup><sup>b</sup>

<sup>1</sup>Department of Electrical and Electronics Engineering, College of Engineering, Koç University, Istanbul, Turkey

<sup>2</sup>Department of Orthopaedics and Traumatology, School of Medicine, Koç University, Istanbul, Turkey  
{ctekdemir21, yhayirlioglu17, olgarbirsnel, besemiz}@ku.edu.tr

**Keywords:** Knee Health, Acoustical Emissions, Electrical Bioimpedance, Inertial Activity, Rehabilitation Monitoring.

**Abstract:** The knee, being the largest and one of the most complex joints in the body, is highly vulnerable to injury due to its intricate structure and exposure to multi-directional forces. Surgical interventions are among the most frequently utilized treatments for advanced degenerative joint disease. However during the rehabilitation process, physician assessments can be subjective, which may lead to inconsistent evaluations, particularly in subtle or complex cases. To enhance accuracy and reduce variability, objective methodologies like data-driven tools and standardized protocols are necessary. Hence, we propose a multi-modal wearable sensor framework leveraging electrical bioimpedance, acoustical emissions, inertial activity and temperature measurements simultaneously to achieve objective and quantifiable information that can complement clinical judgement, ensuring more reliable and reproducible outcomes in patient care. The system was validated through active (flexion-extension) and inactive (sedentary) measurements, and proven successful in capturing knee-related signatures and assessing the knee joint health. Such a system could facilitate the establishment of a direct relationship between signal characteristics and key knee health parameters, enabling more informed decisions regarding disease or injury status and treatment progress.


## 1 INTRODUCTION


The knee is the largest and one of the most complex joints in the human body, making it highly susceptible to stress from multi-directional forces during physical activity (Austermuehle, 2001). Its intricate structure, comprising two distinct joints, accommodates loads from various directions while relying on both static and dynamic soft tissues to maintain stability. This complexity, along with age-related wear and tear, makes the knee particularly vulnerable to injury and a leading cause of rehabilitation among musculoskeletal disorders. Globally, an estimated 1.71 billion people suffer from musculoskeletal conditions, a number projected to rise with an aging population (WHO, 2022).

Surgical interventions are one of the most commonly used treatment approaches for advanced degenerative joint disease. Indeed, the number of total knee arthroplasties performed each year in the United States alone is estimated to reach 3.5 million

in 2040 (Carmichael et al., 2022). Following surgery, the main goal in the early postoperative period is to maintain proper healing of the surgical wound. This process is monitored by simple observation and physical examination findings. Healing, which begins as soon as the surgical incision is made, should follow a decrease in soft tissue edema, redness and temperature, finally leading to restoration of skin integrity (George Broughton et al., 2006). The second important point is to restore the range of motion of the knee joint, which is calculated through angular values while the physician is passively moving the knee joint or asking the patient to actively bend the knee. The physician can then conclude whether the wound is healing smoothly in the early postoperative period and the inflammatory process has regressed as expected – or can make necessary interventions and provide warnings by identifying disruptions in the natural course of recovery.

One problem with the physician assessments is their subjectivity as they often rely on personal experience, intuition and observation, which can vary between individuals and lead to inconsistent evaluations, especially in subtle or complex cases. To

<sup>a</sup>  <https://orcid.org/0000-0002-2137-1164>

<sup>b</sup>  <https://orcid.org/0000-0002-7544-5974>

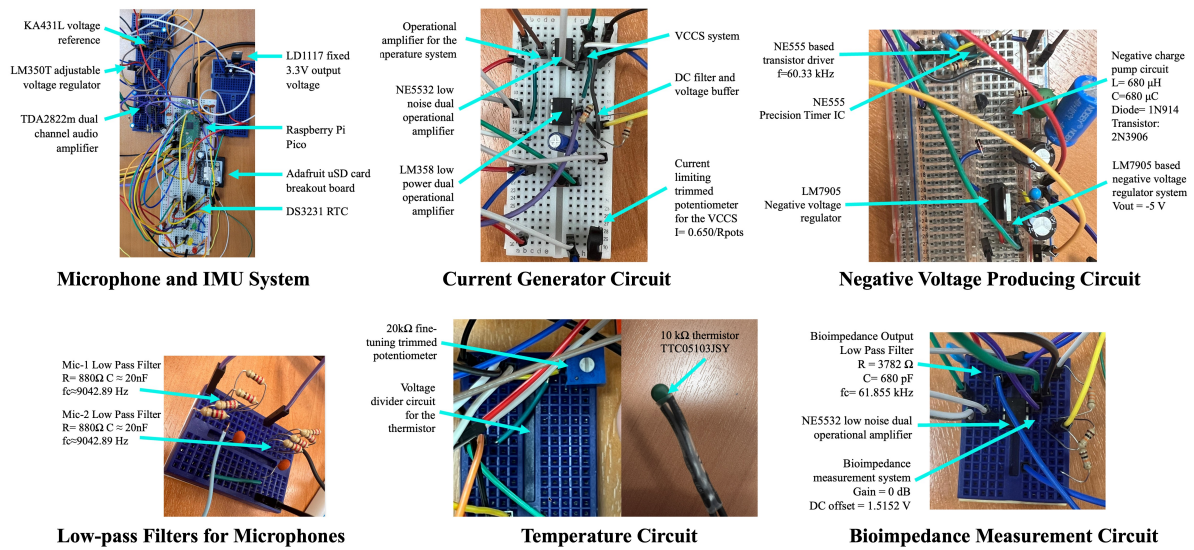


Figure 1: Most important circuit components.

reduce variability and improve accuracy, objective methodologies, such as data-driven tools and standardized protocols, are required. In the literature, several attempts have been made to assess knee health non-invasively which are expected to provide patients and physicians with more readily available quantitative data regarding health or treatment status. Most of these attempts have focused on the design of wearable sensing modalities leveraging the measurement of joint acoustics, edema or activity range through miniature microphones, electrical bioimpedance (EBI) systems and inertial measurement units (IMUs), respectively. For example, joint acoustics (vibrations emitted from the mid-patella during active movements) have been used to distinguish between subjects with osteoarthritis and healthy subjects (Sarillee et al., 2014), to track treatment and medication effectiveness in children with arthritis (Semiz et al., 2018) and to monitor rehabilitation advancements in athletes with an acute injury (Hersek et al., 2017). On the other hand, several studies have leveraged the use of EBI in joint edema (swelling) detection and monitoring (Hersek et al., 2016); and IMUs for knee joint stability (Kianifar et al., 2017) and range of motion assessment (Seel et al., 2014).

In this work, we propose a multi-modal sensor system prototype leveraging electrical bioimpedance, acoustical emissions, inertial activity and temperature measurements simultaneously to achieve objective and quantifiable information that can complement clinical judgement, ensuring more reliable and reproducible outcomes in patient care. Such a multi-modal system could potentially facilitate the investigation of

one-to-one correspondence between signal characteristics and important knee health parameters, enabling more informed decisions regarding the disease/injury state or treatment progression.

## 2 METHODS

### 2.1 Hardware Setup

In the system, a Raspberry Pi Pico based on RP2040 microcontroller is used as the development kit. The circuit visuals are provided in Figure 1 and the sensor locations are visualized in Figure 2. The system has two modes: an active mode and an inactive (passive) mode. In the active mode, acoustical emissions and inertial activity measurements are employed, whereas during inactive mode, the electrical bioimpedance and temperature values are measured. Details regarding electrical bioimpedance, temperature, acoustical emissions and inertial activity are presented in the upcoming sub-sections.

#### 2.1.1 Electrical Bioimpedance Measurement System

The bioimpedance system uses an AD9833 signal generator module to generate a 60 kHz sine wave with an amplitude and DC offset of 325 mV each. Subsequently, this generated signal is fed into a DC offset remover and voltage buffer circuit (which uses an LM358 op-amp) to be turned into a pure AC signal. The output from the LM358 circuit is then fed into

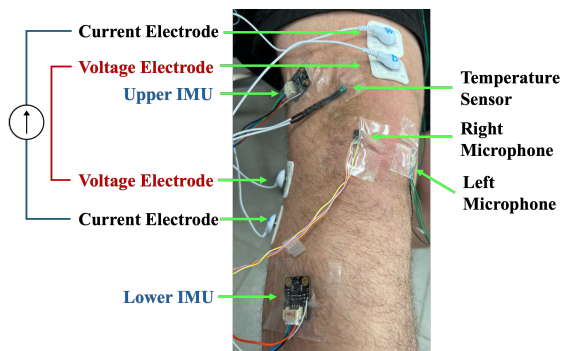


Figure 2: Sensors included in the system.

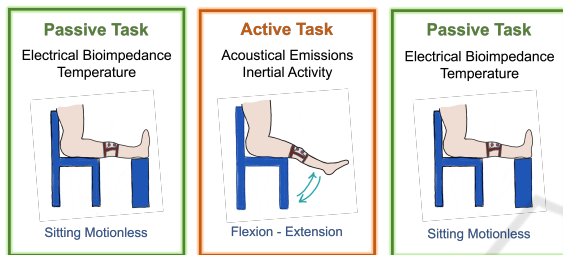


Figure 3: Experimental protocol including active and inactive (passive) measurements.

a NE5532 op-amp based VCCS (Voltage Controlled Current Source) circuit. The VCCS circuit sends out a constant 2 mA peak-to-peak current from the op-amp's output pin to its inverting input pin. The leg electrodes are connected to these pins to send a constant AC current through the knee joint. Additionally, the VCCS circuit uses a potentiometer to fine-tune the magnitude of the AC current.

The voltage across the knee joint is measured with an NE5532 op-amp based circuit. The circuit consists of a simple inverting summing amplifier (which uses the NE5532) and a low-pass filter. The top-leg electrode's potential acts as the input signal, while the bottom-leg's is connected to the ADC ground (which makes it act as a reference ground for the system). The circuit adds the input voltage and a voltage source of -1.5151 volts (which is half of the reference voltage of the RP2040's ADC) together, inverts the signal (so that it is positively shifted for the ADC), and then feeds it into an anti-aliasing (low pass) filter, which then gets connected to one of the ADC pins on the Pico. It should be noted that the output signal is not too large to cause any clipping or go beyond the ADC's range, which is why this level of DC offset is perfectly adequate for the Pico's ADC.

The negative voltage producing circuit consists of a NE555 precision timer-based square wave generator that drives a negative charge-pump circuit and a LM7905 negative voltage regulator. The system functions by continuously driving a negative charge-

pump circuit at 60.33 kHz. The negative charge-pump circuit consists of a 680  $\mu\text{H}$  inductor, a 1N914 fast switching diode, a 680  $\mu\text{F}$  capacitor, and a 2N3906 PNP BJT transistor to act as a switch. At 60.33 kHz, the charge-pump circuit produces a stable -11.5 volts while being able to deliver a current around -6.8 mA. The output from the charge-pump circuit is then fed into a LM7905 negative voltage regulator, which reduces and stabilizes the negative voltage circuit's output to -5 volts. The negative voltage producing circuit's output is primarily used in powering all of the op-amps found in the system. It is also used as a constant offset voltage for the aforementioned bioimpedance voltage measurement system.

### 2.1.2 Temperature Measurement System

The temperature measurement circuit is based on a voltage divider that consists of a thermistor and a resistor. A 10 k $\Omega$  negative-thermal-coefficient thermistor (model: TTC05103JSY) is connected in series with a 10 k $\Omega$  resistor. As the thermistor's temperature increases, its resistance decreases, which causes the voltage across the 10 k $\Omega$  resistor to increase. The output voltage on the resistor is fed into a NE5532 op-amp based voltage buffer and the output of the voltage buffer is fed into a low pass filter with a frequency cutoff of 15.92 Hz. It should be noted that the temperature on the thermistor changes very slowly due to thermodynamic phenomena and that the DC component of the output signal is significantly more important than the AC component. Therefore, the low-pass filter is implemented to function as a pseudo-AC filter that also blocks off power-line interference and other unneeded higher frequencies. The NE5532 is used as a buffer to preserve the voltage so that the voltage divider's output is not affected due to the low pass filter. The output of the filter is fed into the Pico's second ADC pin to calculate the thermistor's temperature. It should also be noted that the voltage-to-temperature calculation is done internally in the Pico itself.

### 2.1.3 Acoustical Emissions System

Two miniature Knowles BU-23173 analog contact microphones were used in the acoustic emission system. Both microphones were amplified through the TDA2822m audio amplifier integrated with 39 dB gain. After amplification, the signals are passed through an anti-aliasing filter. Since the sampling rate used in the microphones was 20 kHz, this results in a Nyquist frequency of 10 kHz; hence, two first-order low-pass filters with a cut-off frequency of 9042.89 Hz are used to avoid aliasing during the recordings.

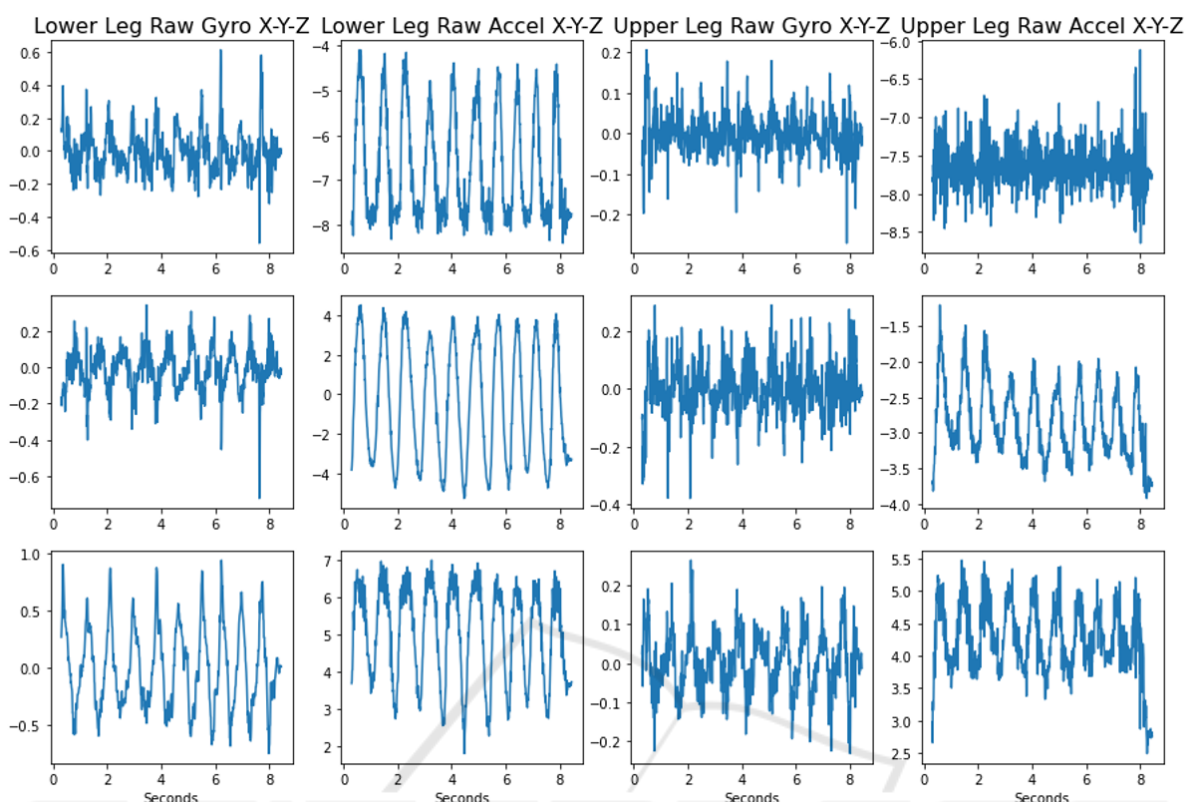


Figure 4: Raw IMU measurements showing accelerometer and gyroscope recordings individually.

### 2.1.4 Inertial Activity System

The inertial activity system measures joint motion and angular changes along with knee acoustical emissions during active movements. Accordingly, 2 IMU sensors are included in the system, one fixed to the thigh (upper) and the other to the calf (lower). A 6-axis (3-axis accelerometer and 3-axis gyroscope) digital BMI160 sensor is selected as the IMU. Each of the IMUs receives data with a sampling rate of 100 Hz. The raw accelerometer and gyroscope data are then used for direction/angle calculation via quaternions.

### 2.1.5 Final System Design

In addition to the individual systems described above, various peripheral elements are also used in the design.

The system switches between “active” and “inactive” measurements via a DPDT (double pole, double throw) switch that is controlled externally. When the switch is in the “active” measurement position, the output signals from the inertial activity system and the acoustical emissions system are fed into the Pico’s ADC pins. When the switch is set into the “passive” position, the outputs from the electrical bioimpedance system and the temperature measurement system are

fed into the ADC pins instead. This way, only one set of measurements are taken at a time.

When the switch is in “active” mode, three different buttons are used to toggle between the “Start”, “Hold” and “Stop” commands. When the recording starts, a file is created on the microSD card for the active mode; where the acoustic emission signals and IMU data are recorded into this file. The files are named using the date and time information captured via the DS3231 RTC module. A flag is also added to the file name to indicate that the record is an “active” record.

When switching to “inactive” mode using the switch, a second start button is used to create a separate file with a different flag (note that the file name still uses the date and time information from the DS3231). Although a second “Start” button is used for this mode, it shares the same “Hold” and “Stop” buttons. This mode measures only 2 signals; namely the electrical bioimpedance and the temperature, which are both analog signals. The voltage-to-temperature measurement is done internally (as mentioned before), and the measured skin voltage is saved directly into the file. All of the recorded measurement data is saved onto an SD card through a Adafruit microSD card module.



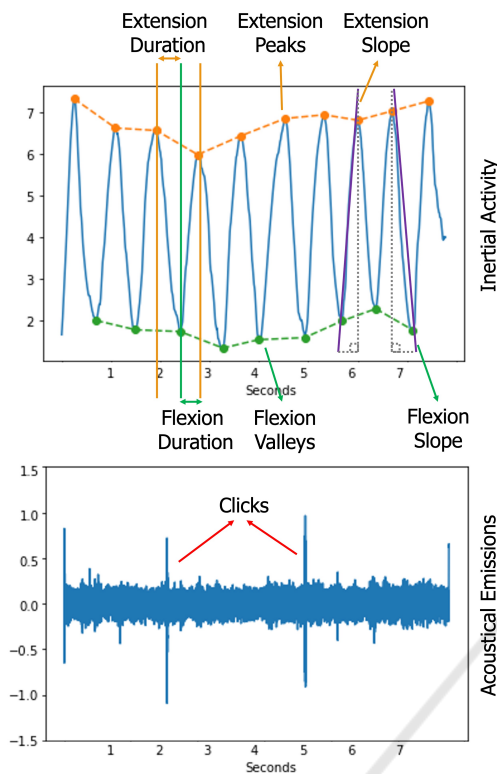


Figure 5: IMU-derived angle and acoustical emission signals shown together.

Additionally, there are 3 LEDs in the system that indicate whether the system is functioning properly. The green LED lighting up indicates that the recording is running smoothly (for the “active” mode), while a red LED indicates that there is a problem with the system (e.g. SD card non-contact). For the “inactive” mode, both the green and the yellow LED light up to indicate that the system is recording.

## 2.2 Data Collection and Experimental Protocol

The protocol for the measurements basically consists of two main parts: (i) the sedentary recording part during rest and (ii) the active recording part including active tasks, as seen in Figure 3. Data was collected from a healthy male participant in laboratory settings. First, bioimpedance and temperature values were measured during 20 seconds of sedentary measurement, followed by the active period. During the active period, 10 flexion-extension exercises were performed, during which the corresponding inertial activity and acoustic emission measurements were taken. The protocol was terminated with a second 20-second sedentary period.

## 2.3 Analysis Framework

### 2.3.1 Electrical Bioimpedance Analysis

The recorded bioimpedance signal was analyzed with a simple signal processing algorithm implemented in Matlab. First, the signal was passed through a very tight band-pass filter ([59.5, 60.5] kHz) and then multiplied by 41.1392. This scaling value was obtained experimentally: The output of the function generator was fed as an input to the bioimpedance measurement circuit and then the amount of drift and noise was analyzed. It was observed that the use of a bandpass filter and this scaling factor resulted in a signal very close to the signal seen on the oscilloscope. This algorithm prevents any external noise from passing through and also makes the calculated knee impedance more accurate.

### 2.3.2 Temperature Analysis

For the temperature measurement, the Pico was programmed to shift the incoming data by 13 bits before any value was calculated. The main reason behind this is to avoid noise interference and to compensate for the voltage difference between the output of the filter and the output of the voltage divider. In addition, a simple compression algorithm was used to reduce the temperature range to [24.5, 50.0] degrees Celsius. Following the compression algorithm, the temperature was shifted down to eliminate the added bits and any DC noise.

### 2.3.3 Inertial Activity Analysis

The raw accelerometer and gyroscope data recorded on the SD card were first filtered between 0.1 Hz and 48 Hz using a finite impulse response (FIR) Kaiser window band-pass filter. The triaxial accelerometer and gyroscope signals recorded from the calf (lower) and thigh (upper) regions for each IMU of a sample subject are visualized in Figure 4.

The raw accelerometer and gyroscope data were then evaluated for direction/angle calculation using quaternions (Seel et al., 2014). Accordingly, an extended Kalman filter was used to estimate an orientation represented as a quaternion. The algorithm first estimates the new state (the most recent orientation) for the calf and thigh using the instantaneous measurements of the gyroscopes, then makes the necessary corrections using the measurements of the accelerometers. Next, quaternions are extracted from the calculated orientations for the calf and thigh and rotation matrices are calculated for both regions. These two rotation matrices are multiplied to obtain

Table 1: The calculated inertial activity characteristics.

	Flexion Time	Flexion Range	Flexion Slope	Extension Time	Extension Range	Extension Slope
<b>Mean</b>	0.417	4.966	0.121	0.382	4.959	0.133
<b>Std</b>	0.051	0.267	0.015	0.064	0.381	0.021
<b>Max</b>	0.510	5.345	0.138	0.540	5.517	0.172
<b>Min</b>	0.360	4.543	0.091	0.320	4.261	0.099

the relative rotation. Finally, from this relative rotation matrix, relative angle values in x, y and z directions are obtained through Euler transformation.

The relative angles x, y and z represent the relative roll, pitch and yaw signals respectively. For angle tracking and the extraction of relevant features, relative pitch graph was used in accordance with the mechanical orientations. On the relative pitch graph, several features were calculated. First, the peak amplitudes, durations and slopes were extracted for each flexion or extension movement. Then, the mean, standard deviation, minimum, and maximum values of the peak, duration, and slope of all cycles were calculated to evaluate the irregularity of the exercises, as well as the maximum and minimum angles reached. It should be noted that the features were extracted from the non-normalized signal. This would potentially enable the assessment of the maximum/minimum angle differences between the participants in future studies.

### 2.3.4 Acoustical Emissions Analysis

The .bin files saved on the SD card were first converted to the appropriate format using Matlab. It should be noted that the following pre-processing and feature extraction steps were repeated for both the left and right microphones. First, hardware noise was suppressed using narrow band-stop filters ([185, 205] and [940, 1050] Hz). The remaining pre-processing and feature extraction steps were then employed in Python (version 3.11).

In order to extract the clinically relevant part of the acoustic emission data from the microphones, a finite impulse response (FIR) Kaiser window bandpass filter between 250 Hz and 5 kHz was used. An example signal is presented in Figure 5. In order to visualize that the system successfully captures the felt clicks, a signal containing clicks was specifically selected.

The signal was then divided into 500 ms windows in parallel with the studies in the literature and 250 ms overlap was used between the subsequent windows (50% overlap). For the two different window types (with and without clicks), we reported the distinctive differences in the features selected from 3 different groups: temporal (peak-to-peak), statistical (kurtosis) and spectral (roll-off).

## 3 RESULTS AND DISCUSSION

### 3.1 Inertial Activity and Acoustical Emissions Results

As mentioned in Section 2.2, the participant performed 10 flexion-extension exercises during the pilot data acquisition. Figure 5 clearly shows the angular change. The dots on the graph represent the moments of flexion, while the peaks represent the moments of maximum extension. Although the preliminary analysis focused on angular features, direct analysis of raw accelerometer and gyroscope data would also be possible in the long term due to their high signal quality. In addition, the peak amplitudes, durations and slopes were extracted for each flexion or extension movement. Then, the mean, standard deviation, minimum, and maximum values of the peak, duration, and slope of all cycles were calculated to evaluate the irregularity of the exercises, as well as the maximum and minimum angles reached. The derived values are presented in Table 1.

Figure 6 shows a superimposition of 500 ms (10000 samples)-long segments, and examples of a silent window and a window with clicks. As explained in Section 2.3.4, three different features were extracted from a sample silent window and a window with clicks. As seen, the peak-to-peak values were 0.081 and 0.023; whereas the kurtosis values were 26.863 and 0.628, respectively. As higher kurtosis refers to the presence of more extreme values or outliers (i.e. tailedness) compared to a normal distribution, it was indeed aligning with the morphology differences between a window with click and a silent window. Similarly, the spectral roll-off values were calculated to be 0.988 and 0.628, respectively. Higher spectral roll-off in signal analysis indicates that a greater proportion of the signal's energy is concentrated in the higher frequency components. The joint clicks are characterized by high energy and short duration, typically lasting between 10 and 20 milliseconds. Furthermore, these emissions contain high-frequency components, with bandwidths extending up to 20 kHz, a range commonly expected for acoustic emissions (Teague et al., 2016). Hence, hav-

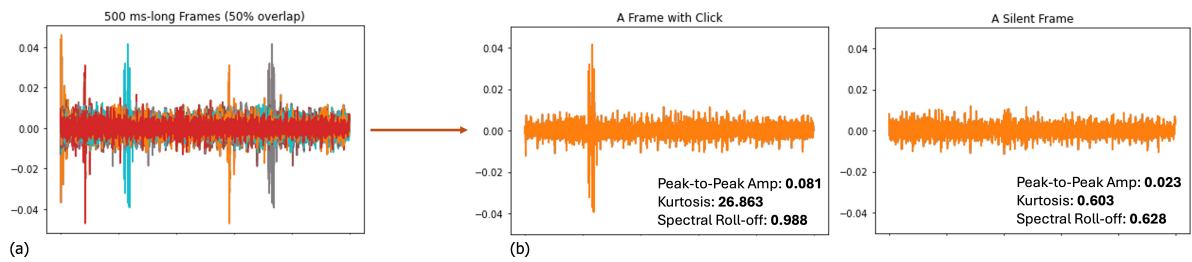


Figure 6: (a) Superimposition of acoustical emission frames. (b) Examples of a frame with a click and a silent frame.

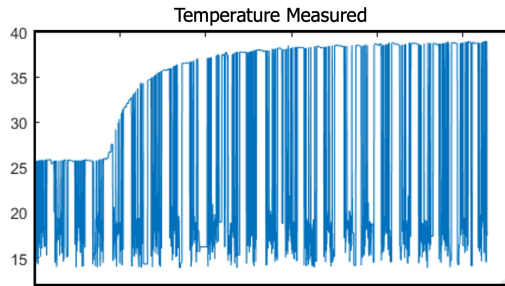


Figure 7: Temperature measurement.

ing a higher spectral roll-of value indeed aligns with the literature.

### 3.2 Temperature and Bioimpedance Results

The temperature and impedance measurement analyses were explained in Sections 2.3.2 and 2.3.1, respectively. Accordingly, the resulting temperature measurement for the participant is presented in Figure 7. Similarly, the impedance value was calculated to be 97.9246 Ohm. This value was indeed in line with the impedance values of healthy knees in studies in the literature (Hersek et al., 2015).

## 4 CONCLUSION

In this work, we presented a multi-modal wearable sensor framework leveraging electrical bioimpedance, acoustical emissions, inertial activity and temperature measurements simultaneously to obtain objective and measurable information that can support clinical decision-making. The system was validated using active (flexion-extension) and inactive (sedentary) measurements and proven to be successful in measuring the knee-related parameters.

The main limitation of the current design is the extensive number of components. Hence, future work will focus on transforming the current design into a printed-circuit-board (PCB) and validating it in actual clinical settings more easily. The first potential use

area will be to monitor the rehabilitation period of the patients undergone total knee arthroplasty. Such a system could help establishing direct relationships between signal characteristics and key knee health parameters, allowing for more informed decisions about the disease or injury status and treatment progress.

## ACKNOWLEDGEMENTS

This work was supported by the Health Institutes of Turkiye (TUSEB) under grant number 22554.

## REFERENCES

- Austermuehle, P. D. (2001). Common knee injuries in primary care. *The Nurse Practitioner*, 26(10):26–32.
- Carmichael, J., Dennis, D., Jennings, J., Stevens-Lapsley, J., and Bade, M. (2022). Feasibility and initial efficacy of a multimodal swelling intervention after total knee arthroplasty: A prospective pilot study with historical controls. *The Knee*, 35:25–33.
- George Broughton, I., Janis, J. E., and Attinger, C. E. (2006). Wound healing: an overview. *Plastic and reconstructive surgery*, 117(7S):1e–S.
- Hersek, S., Pouyan, M. B., Teague, C. N., Sawka, M. N., Millard-Stafford, M. L., Kogler, G. F., Wolkoff, P., and Inan, O. T. (2017). Acoustical emission analysis by unsupervised graph mining: A novel biomarker of knee health status. *IEEE Transactions on Biomedical Engineering*, 65(6):1291–1300.
- Hersek, S., Töreyn, H., and Inan, O. T. (2015). A robust system for longitudinal knee joint edema and blood flow assessment based on vector bioimpedance measurements. *IEEE Transactions on biomedical circuits and systems*, 10(3):545–555.
- Hersek, S., Töreyn, H., Teague, C. N., Millard-Stafford, M. L., Jeong, H.-K., Bavare, M. M., Wolkoff, P., Sawka, M. N., and Inan, O. T. (2016). Wearable vector electrical bioimpedance system to assess knee joint health. *IEEE Transactions on Biomedical Engineering*, 64(10):2353–2360.
- Kianifar, R., Lee, A., Raina, S., and Kulić, D. (2017). Automated assessment of dynamic knee valgus and risk of knee injury during the single leg squat. *IEEE journal*

*of translational engineering in health and medicine*, 5:1–13.

- Sarillee, M., Hariharan, M., Anas, M., Omar, M., Aishah, M., and Oung, Q. W. (2014). Assessment of knee joint abnormality using acoustic emission sensors. In *2014 IEEE International Conference on Control System, Computing and Engineering (ICCSCE 2014)*, pages 378–383. IEEE.
- Seel, T., Raisch, J., and Schauer, T. (2014). Imu-based joint angle measurement for gait analysis. *Sensors*, 14(4):6891–6909.
- Semiz, B., Hersek, S., Whittingslow, D. C., Ponder, L. A., Prahalad, S., and Inan, O. T. (2018). Using knee acoustical emissions for sensing joint health in patients with juvenile idiopathic arthritis: A pilot study. *IEEE sensors journal*, 18(22):9128–9136.
- Teague, C. N., Hersek, S., Töreyn, H., Millard-Stafford, M. L., Jones, M. L., Kogler, G. F., Sawka, M. N., and Inan, O. T. (2016). Novel methods for sensing acoustical emissions from the knee for wearable joint health assessment. *IEEE Transactions on Biomedical Engineering*, 63(8):1581–1590.
- WHO (2022). Musculoskeletal health — who.int. World Health Organization. [Accessed 06-10-2024].

